J|A|C|S ARTICLES

Published on Web 08/03/2010

Assessing Molecular Transport Properties of Nanoporous Materials by Interference Microscopy: Remarkable Effects of Composition and Microstructure on Diffusion in the Silicoaluminophosphate Zeotype STA-7

Despina Tzoulaki,*,‡ Lars Heinke,§ Maria Castro,⊥ Pablo Cubillas,# Michael W. Anderson,# Wuzong Zhou,|| Paul A. Wright,*,|| and Jörg Kärger†

Department of Experimental Physics I, University of Leipzig, Linnestrasse 5, 04103, Leipzig, Germany, Technische Chemie II, Technische Universität München, Lichtenbergstrasse 4, 85747 Garching, Germany, Fritz-Haber-Institute der Max-Plank-Gesellschaft, Faradayweg 4-6, 14195 Berlin, Germany, School of Chemistry, University of St. Andrews, North Haugh, St. Andrews, Fife, KY16 9ST Scotland, United Kingdom, IFP-Lyon, BP. 3, 69390, Vernaison, France, and Centre for Nanoporous Materials, School of Chemistry, The University of Manchester, Oxford Road, Manchester, M13 9PL United Kingdom

Received May 11, 2010; E-mail: despina.tzoulaki@tum.de; paw2@st-andrews.ac.uk

Abstract: The influence of the chemical composition and of the storage and activation protocol on the diffusion of methanol into strongly chemically zoned crystals of the silicoaluminophosphate zeotype STA-7 has been investigated by interference microscopy. Analysis of the evolution of transient intracrystalline concentration profiles reveals that just-calcined SAPO STA-7 crystals with lower Si content (Si/(Si + P) = 0.18) exhibit higher surface permeability and bulk diffusivity than those with higher Si content (S/(Si + P) = 0.37). Remarkably, crystals with the higher Si content which were stored in the calcined form crack during activation along planes of weakness already present in the as-prepared crystals, creating fresh surfaces through regions of lower Si that are much more easily penetrated by the adsorbing methanol than are the original surfaces.

Introduction

In many cases of practical application, including catalytic transformations and adsorptive separations, the functionality of porous materials[1] depends on their transport properties, which are in turn determined by their structure. The performance of real materials in these applications is subject to many influences,[2] often resulting from their significant deviation from perfect crystal structure.[3] For instance, recent studies with ZSM-5 crystals report a correlation between their morphology and their molecular diffusion barriers.[4] By monitoring diffusion paths with lengths extending to the dimensions of the host particles, interference microscopy[5,6] is ideally suited to the exploration of transport phenomena in such materials. Observing the evolution of guest profiles with a spatial resolution of 0.5 μm, it reveals the transport characteristics of nanoporous host materials more clearly than any previous method. Using methanol as a probe molecule, we illustrate the power of this technique by demonstrating the remarkable sensitivity of the transport properties of the silicoaluminophosphate zeotype STA-7[7,8] to its framework composition and also to the route by which the microporous solid is prepared and activated.

SAPO STA-7 belongs to a family of polytypic aluminophosphate-based solids constructed entirely of double 6-membered ring building units. Different amounts of silicon atoms can be introduced into the $AlPO_4$ framework, and solid state NMR of the as-prepared materials shows that in the materials examined in this study all silicon is included by replacement of phosphorus atoms, so that in the framework there is strict alternation of Al with P or Si in the tetrahedral cations sites.[9] In the present paper, we report results considering STA-7 samples prepared from gels with two different starting compositions. The bulk Si/(Si + P) values of the (P,Si) framework sites of the final crystalline products were measured as 0.18 (for SAPO(10)) and 0.37 (for

‡ Technische Universität München.
§ Fritz-Haber-Institute der Max-Plank-Gesellschaft.
⊥ IFP-Lyon.
The University of Manchester.
|| University of St. Andrews.
† University of Leipzig.

(1) Schüth, F.; Sing, K. S. W.; Weitkamp, J. In *Handbook of Porous Solids*; Wiley-VCH: Weinheim, 2002.
(2) Navrotsky, A. *Nat. Mater.* **2003**, *2*, 571–572.
(3) Ruthven, D. M.; Brandani, S.; Eic, S. M. In *Adsorption and Diffusion*; Karge, H. G., Weitkamp, J., Eds.; Springer: Berlin, Heidelberg, 2008.
(4) Karwacki, L.; et al. *Nat. Mater.* **2009**, *8*, 959.
(5) Kärger, J.; Kortunov, P.; Vasenkov, S.; Heinke, L.; Shah, D. B.; Racozky, R. A.; Traa, Y.; Weitkamp, J. *Angew. Chem., Int. Ed.* **2006**, *45*, 7846.
(6) Heinke, L.; Tzoulaki, D.; Chmelik, C.; Hibbe, F.; van Baten, J. M.; Lim, H.; Li, J.; Krishna, R.; Kärger, J. *Phys. Rev. Lett.* **2009**, *102*, 065901.
(7) Heinke, L.; Kortunov, P.; Tzoulaki, D.; Castro, M.; Wright, P. A.; Kärger, J. *Europhys. Lett.* **2008**, *81*, 26002.
(8) Castro, M.; Garcia, R.; Warrender, S. J.; Slawin, A. M. Z.; Wright, P. A.; Cox, P. A.; Fecant, A.; Mellot-Draznieks, C.; Bats, N. *Chem. Commun.* **2007**, 3470.
(9) Castro, M.; Warrender, S. J.; Wright, P. A.; Apperley, D. C. *J. Phys. Chem. C* **2009**, *113*, 15731.

SAPO(30)) by ICP-MS analysis (Sample codes SAPO(10) and SAPO(30) indicate that Si/(Si + P) ratios in the synthesis gel were 0.1 and 0.3, respectively).

Silicoaluminophosphate (SAPO) STA-7 crystals have high porosity and a three-dimensional connectivity through small pores around 4 Å in free diameter. Like its polytype SAPO-34, which is a promising catalyst for the industrially important conversion of methanol to ethene and propene (methanol-to-olefins, MTO),[10−13] SAPO STA-7 is an active and stable catalyst for this reaction.[9] Recently, Mores et al.[14] and Karwacki et al.[15] visualized physicochemical processes in single SAPO-34 crystals, such as coke deposition during MTO conversion and thermal decomposition of template, in a space- and time-resolved manner using microspectroscopy combined with optical microscopy.

Materials and Methods

Crystals of the silicoaluminophosphate forms of STA-7 were prepared and characterized according to published methods and techniques.[8,9] The surfaces of crystals of SAPO(30) STA-7 that by optical microscopy showed well-defined planes passing through across their centers were investigated by atomic force microscopy, using methods described previously to investigate growth of SAPO STA-7.[16]

To determine whether the STA-7 crystals have uniform composition or are compositionally zoned, samples were embedded in a block of epoxy resin, and once this had hardened, the block was sliced and polished to obtain sections through single crystals. The freshly exposed surface was coated with a thin layer of gold by sputtering, to avoid charging in the electron microscope. Specimens of SAPO(10) and SAPO(30) prepared in this way were analyzed by selected area EDX in a JEOL JSM-5600 scanning electron microscope, using a voltage of 15 kV and a spot size of ca. 50 nm. This results in an interaction volume with a diameter of ca. 1 μm. It was not possible from the contrast to determine whether crystals had been cut through or whether they were still fully embedded in the resin. Therefore, in order to be sure that the surface exposed to electrons results from the slicing through a crystal, crystals with triangular or trapezoidal silhouettes were carefully examined (examples of the SEM images of such crystals, together with a schematic explanation of their observed geometries and the selected area sampling, are given in Figure 2). Although the centers of the crystals were not analyzed by measuring on triangular or trapezoidal surfaces prepared by this method, zoning effects toward the outer surface were clearly observed. The composition at the crystal center would be less than the minimum value observed at the center of the section, as suggested by extrapolation of our measurements. By simple geometric considerations, the sections were estimated to extend around two-thirds of the way to the crystal center. In the analyses, there was partial overlap of the emitted Au Mα X-ray peak (from the gold coating) with the emitted P K_α X-ray peak from the sample, so the atomic Si/Al ratio is reported. ^{29}Si MAS NMR of these materials in the as-prepared form indicates all Si is in the 'P' site, so the Si/Al ratio should be similar to the Si/(Si + P) ratio.

To render the SAPO STA-7 crystals porous, they were calcined in oxygen at 550 °C for 12 h. This results in removal of the organic templates used in their synthesis (cyclam and tetraethylammonium ions) to give microporous solids that exhibit type I isotherms with pore volumes of 0.29 $cm^3\ g^{-1}$.[8,9]

Prior to study of the uptake of methanol by Interference Microscopy (IFM), calcined samples of STA-7 were activated in situ in the IFM apparatus by removal of adsorbed water. This involved heating the sample to 200 °C with a temperature increase of 1 °C/min and keeping the samples for 10 h at 200 °C, under continued evacuation. Two treatments were adopted for sample SAPO(30): (i) storage of the as-prepared samples in a closed vial in the laboratory for several weeks, with sample calcination in oxygen at 550 °C immediately before the measurements; and (ii) calcination in oxygen at 550 °C immediately after preparation, followed by storage in a closed vial for several weeks, with activation at 200 °C immediately prior to examination via IFM. Only the first procedure (i) was adopted for sample SAPO(10).

The transport properties of nanoporous materials[17,18] are quantified by the (transport) diffusivity D, introduced by Fick's first law

$$j = -D\frac{\partial c}{\partial x} \tag{1}$$

as the proportionality factor between the flux of guest molecules within the host material and their concentration gradient,[19−22] and by the surface permeability α defined as the factor of proportionality between the molecular flux through the surface and the difference between the actual concentration of guest molecules close to the surface (approximately 0.5 μm from the boundary) and the value which, eventually, would be established in equilibrium with the external atmosphere of guest molecules:[19,23]

$$j_{\text{surf}} = \alpha(c_{\text{boundary}} - c_{\text{equilibrium}}) \tag{2}$$

A full description of the experimental techniques applied for the diffusion measurements and the procedures of data analysis is given in the Supporting Information.

^{27}Al and ^{31}P MAS spectra of as-prepared and calcined STA-7 SAPO(30) were obtained using a Varian VNMRS spectrometer operating at 104.20 and 161.88 MHz for ^{27}Al and ^{31}P, respectively. Spectral referencing is with respect to a 1 M $Al(H_2O)_6^{3+}$ solution and an 85% H_3PO_4 solution. One-dimensional ^{27}Al spectra were obtained using direct-polarization from 10000 repetitions with a recycle delay of 0.2 s, ~30° pulse angle, and at a spin-rate of 14 kHz. ^{31}P spectra were obtained in a similar fashion but with a 90° pulse, 120 s recycle delay, and 16 repetitions and 14 kHz spin-rate (refer to Figure S6 in Supporting Information).

Results

Whereas optical microscopy of as-prepared low Si samples (SAPO(10)) showed crystals with uniform relief, the higher Si content crystals (SAPO(30) showed well-defined zoning (Figure 1b,c). In addition, optical microscopy revealed planes running through some of the SAPO(30) crystals close to their centers (Figure 1c). Atomic force microscopy (Figure 1f) of the {100}

(10) Stöcker, M. *Microporous Mesoporous Mater.* **1999**, *29*, 3–48.
(11) Haw, J. F.; Song, W.; Marcus, D. M.; Nicholas, J. B. *Acc. Chem. Res.* **2003**, *36*, 317.
(12) Haw, J. F.; Marcus, D. M. *Top. Catal.* **2005**, *34*, 41.
(13) Hereijgers, B. P. C.; Bleken, F.; Nilsen, M. H.; Svelle, S.; Lillerud, K.-P.; Bjørgen, M.; Weckhuysen, B. W.; Olsbye, U. *J. Catal.* **2009**, *264*, 77.
(14) Mores, D.; Stavitski, E.; Kox, M. H. F.; Kornatowski, J.; Olsbye, U.; Weckhuysen, B. M. *Chem.—Eur. J.* **2009**, *14*, 11320.
(15) Karwacki, L.; Stavitski, E.; Kox, M. H. F.; Kornatowski, J.; Weckhuysen, B. M. *Angew. Chem., Int. Ed.* **2007**, *46*, 7228.
(16) Cubillas, P.; Castro, M.; Jelfs, K. E.; Lobo, A. J. W.; Slater, B.; Lewis, D. W.; Wright, P. A.; Stevens, S. M.; Anderson, M. W. *Cryst. Growth Des.* **2009**, *9*, 4041.
(17) Wang, G.; Johannessen, E.; Kleijn, C. R.; de Leeuw, S. W.; Coppens, M. O. *Chem. Eng. Sci.* **2007**, *62*, 5110.
(18) Kärger, J.; Vasenkov, S. *Microporous Mesoporous Mater.* **2005**, *85*, 195.
(19) Kärger, J.; Ruthven, D. M. In *Diffusion in Zeolites and Other Microporous Solids*; Wiley & Sons: New York, 1992.
(20) Glicksman, M. E. In *Diffusion in Solids*; Wiley: New York, Chichester, 1999.
(21) Mehrer, H. In *Diffusion in Solids*; Springer: Berlin, 2007.
(22) Keil, F. J.; Krishna, R.; Coppens, M. O. *Rev. Chem. Eng.* **2000**, *16*, 71.
(23) Crank, J. In *The Mathematics of Diffusion*; Clarendon Press: Oxford, 1975.

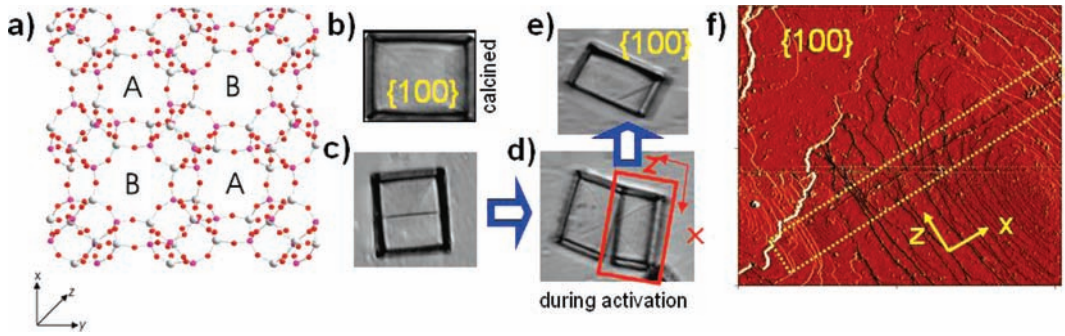

Figure 1. (a) In the structure of SAPO STA-7, two different cages, labeled A and B, alternate. (b) A calcined crystal without observable defect. Panels c−e show the fracturing of a STA-7(30) crystal (stored in the calcined state) with an observed line of weakness into two parts during activation. Notably, in previous studies, STA-7 specimens with lower Si content (Si/(P + Si) = 0.28) stored as-calcined did not lead to fracturing.[7] (f) AFM error image of the {100} surface of an as-prepared STA-7(30) crystal shows the presence of the line of weakness (here in yellow frame). There is no fracturing, though, at this stage, according to the AFM image.

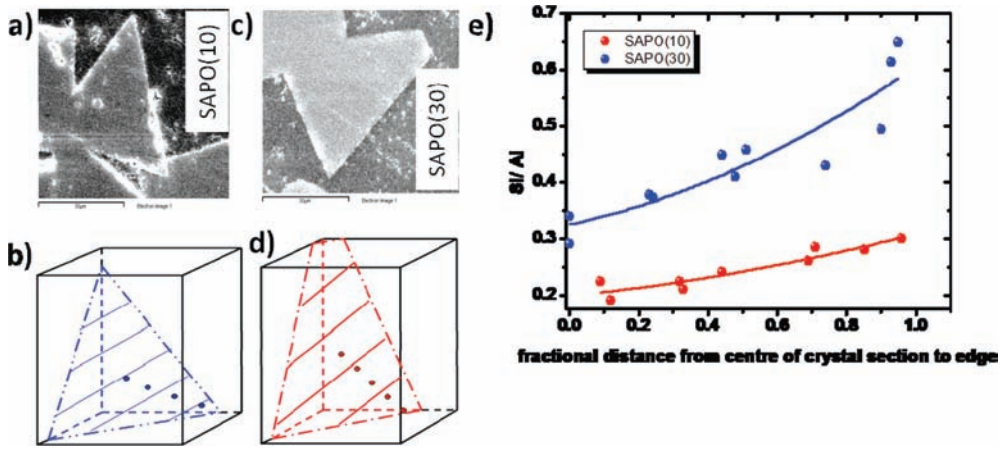

Figure 2. Selected area analyses of sections through crystals. Panels a and c are typical SEM images taken from polished sections of STA-7 crystals embedded in epoxy resin and cut through to give triangular and trapezoidal silhouettes. Panels b and d show how these sections result from cutting through tetragonal prismatic STA-7 crystals, and illustrate schematically where selected area analyses were made. In panel e, the resulting Si/Al ratios are plotted against the distance from the center to the edge of the crystals.

surfaces of as-prepared crystals of the SAPO(30) sample shows the defect plane extends to the outer surface, as well as confirming that the surface is crystalline. As-prepared crystals (synthesized according to refs 8, 9) are never observed to be broken along this plane, but those prepared by procedure (ii), stored in the calcined form and then activated, show fracturing along this plane (Figure 1d,e).

Selected area EDX analyses of sections through SAPO(10) and SAPO(30) crystals (Figure 2e) showed that in each case the Si content increases toward the outer surface. For SAPO(10), the Si/Al ratio increases from 0.19 to 0.30 in the sections, whereas in similar sections of SAPO(30), it increases from 0.29 to 0.65. The Si/Al ratios of the uncut crystal surfaces of SAPO(10) are, therefore, at 0.3, much lower than at the outer surface of the SAPO(30) crystals (0.65) but similar to or higher than that at the central point of the SAPO(30) crystals (by extrapolation, since the measured sections do not go through the crystal centers).

The results and analysis of the IFM measurements of the uptake of methanol in just calcined SAPO(10) and SAPO(30) crystals are described in detail in the ESI. Figure 3a shows a snapshot of the methanol concentration during uptake by a SAPO(10) crystal and Figure 3b the evolution of methanol profiles during adsorption in a SAPO(30) crystal. Both crystals have been calcined immediately prior to adsorption (procedure (i)). In case of SAPO(10), methanol uptake is found to be already in an advanced state only 10 s after the onset of adsorption (the minimum time interval between subsequent profile recording in our present measuring arrangement), and even after this short time interval of time, the boundary concentration is already quite close to its equilibrium value. The increase in silicon content in SAPO(30) strongly retards the uptake, such that the first, clearly observed guest profiles were only established around 270 s after the onset of adsorption, in marked contrast with the behavior of the SAPO(10) crystal. Analysis of the transient concentration profiles on the basis of eqs 1 and 2 (see Supporting Information) yields extremely large surface permeabilities in the case of SAPO(10), close to the upper limit of measurability, with $\alpha_{(10)x} = \alpha_{(10)y} \geq 2.7 \times 10^{-6}$ m s^{-1} and $\alpha_{(10)z} \geq 3.6 \times 10^{-6}$ m s^{-1}. The intracrystalline diffusivities are estimated to be $D_{(10)x} = D_{(10)y} \approx 3.1 \times 10^{-13}$ m^2 s^{-1} and $D_{(10)z} \approx 2.7 \times 10^{-13}$ m^2 s^{-1}, the anisotropy arising from the connection of cages through windows of different sizes along the [100] and [001] directions of the tetragonal structure. For SAPO(30), surface permeabilities of $\alpha_{(30)x} = \alpha_{(30)y} \approx 3.5 \times 10^{-9}$ m s^{-1} and $\alpha_{(30)z} \approx 5.5 \times 10^{-9}$ m s^{-1} and intracrystalline diffusivities of $D_{(30)x} = D_{(30)y} \approx 1.4 \times 10^{-14}$ m^2 s^{-1} and $D_{(30)z} \approx 1.6 \times 10^{-13}$ m^2 s^{-1} have been estimated. Both surface permeability and bulk diffusivity are thus found to decrease strongly with increasing Si content. A summary of all transport

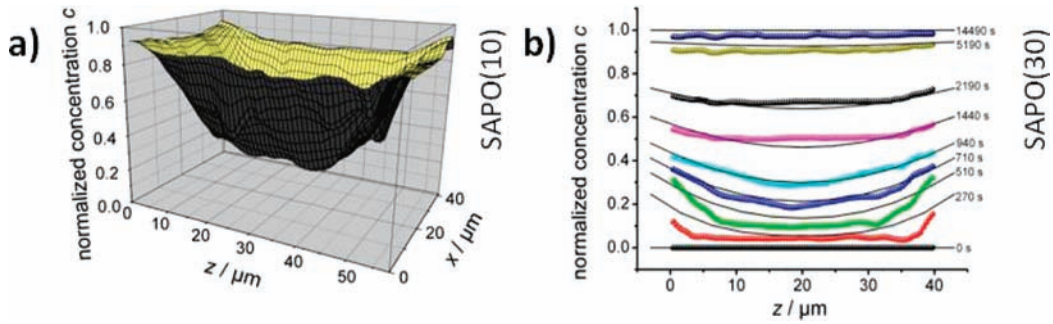

Figure 3. Concentration profiles of methanol during the uptake in (a) the low silica SAPO(10) and (b) the SAPO(30) samples calcined immediately before study. The thin lines show the fits that were achieved with the numerical solutions of the transport equations.

Table 1. Surface Permeabilities and Transport Diffusivities of SAPO STA-7 Samples Investigated in the Present Study and Comparison with the Corresponding Data Obtained in a Previous Study[7] with a Sample of Silicon Content-Intermediate to the Samples Considered in This Study[a]

sample (Si/(Si + P))	surface (mean) permeability α/m s^{-1}	bulk (mean) diffusivity D/m^2 s^{-1}	ref
SAPO STA-7(10) (0.18)	$\geq 2.7 \times 10^{-6}$ ($\alpha_{(10)y} = \alpha_{(10)x}$)	3.1×10^{-13} ($D_{(10)y} = D_{(10)x}$)	This work
Procedure (i)	$\geq 3.6 \times 10^{-6}$ ($\alpha_{(10)z}$)	2.7×10^{-13} ($D_{(10)z}$)	
SAPO STA-7(20) (0.30)	1.2×10^{-8} ($\alpha_{(20)y} = \alpha_{(20)x}$)	5.8×10^{-14} ($D_{(20)y} = D_{(20)x}$)	7
Procedure (ii)	1.5×10^{-8} ($\alpha_{(20)z}$)	1×10^{-13} ($D_{(20)z}$)	
SAPO STA-7(30) (0.37)	3.5×10^{-9} ($\alpha_{(30)y} = \alpha_{(30)x}$)	1.4×10^{-14} ($D_{(30)y} = D_{(30)x}$)	This work
Procedure (i)	5.5×10^{-9} ($\alpha_{(30)z}$)	1.6×10^{-13} ($D_{(30)z}$)	
SAPO STA-7(30) (0.37)	$\alpha^{\text{fragment}}_{(30)z,\text{ fracture}} = 5 \times 10^{-7}$	$D^{\text{fragment}}_{(30)z} = 6.7 \times 10^{-14}$	This work
Procedure (ii)	$\alpha^{\text{fragment}}_{(30)z,\text{ genuine}} \leq 10^{-9}$		

[a] The arithmetic mean values are listed, since all quantities vary with concentration. The high accuracy of the determined parameters is assured by the reproducibility of the experiments and by the fitting of numerous concentration profiles with only a few free parameters.

parameters (diffusivities and surface permeabilities) determined for silicoaluminophosphate STA-7 samples is given in Table 1.

In separate experiments, SAPO(30) crystals which were stored for several weeks in the calcined form (preparation procedure (ii)) display the remarkable behavior recorded in Figure 1c−e, in which the crystals fracture upon activation. For those crystals, Figure 4 shows the profiles of transient concentration, integrated in the observation direction, during the uptake of methanol on such crystal halves. Methanol uptake is immediately recognized to occur almost exclusively through the freshly created face. Crystal fracture has created a lower Si content surface which is much more easily penetrable than the 'old' crystal surface! By a quantitative assessment of the transient concentration profiles[7,24] (see Supporting Information), the permeability through the fractured face ($\alpha^{\text{fragment}}_{(30)z,\text{fracture}} \approx 5 \times 10^{-7}$ m s^{-1}) is found to exceed the permeability through the genuine crystal boundary ($\alpha^{\text{fragment}}_{(30)z,\text{genuine}} \leq 10^{-9}$ m s^{-1}) by more than 2 orders of magnitude. Simultaneously, intracrystalline diffusivity is estimated to be $D^{\text{fragment}}_{(30)z} \approx 6.7 \times 10^{-14}$ m^2 s^{-1}. Furthermore, uptake close to the crystal edges (along the z direction, Figure 4a) is found to be strongly retarded, indicating decreasing surface permeabilities and/or diffusivities toward the edges.

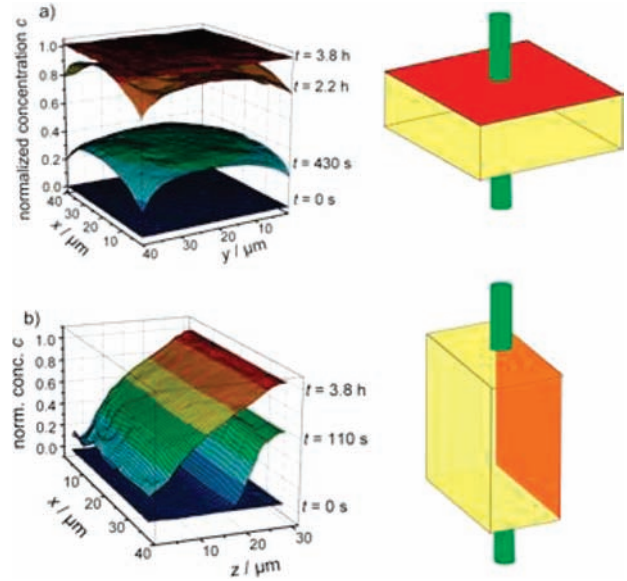

Figure 4. Concentration profiles of methanol during uptake in the fractured crystal. The orientation of the crystals is indicated schematically to the right: The novel (fractured) crystal face, perpendicular to the [001] direction (indicated in red/orange), is (a) perpendicular and (b) parallel to the observation direction (represented in green). In agreement with our expectation, observation perpendicular to the fracture face reflects the isotropic symmetry of the host system in the *xy*-plane, as required by the tetragonal crystal structure. The impressive impact of crystal fracture on its transport properties is revealed by observing molecular uptake after a 90° rotation of the crystal.

Discussion

Comparing the measurements on the methanol uptake of the SAPO STA-7 materials after procedure (i), it is clear that the higher Si solid (SAPO(30)) has both lower surface permeability and lower bulk diffusivity than SAPO(10) (Table 1). The change in surface permeability is particularly marked, being around 3 orders of magnitude. Analysis of methanol adsorption through the freshly fractured surface produced by procedure (ii) on the SAPO(30) sample shows that the surface permeability of the fractured surface is much higher than that of the external surface of the freshly calcined sample. This is attributable to the lower Si content of the center of the crystal (through which part of the fracture plane cuts) than at the original surface: the Si/Al ratio of the center of the crystal is lower than 0.3, whereas the Si/Al ratio of the external surface is ca. 0.6. In addition, an

(24) Heinke, L.; Kärger, J. *New J. Phys.* **2008**, *10*, 023035.

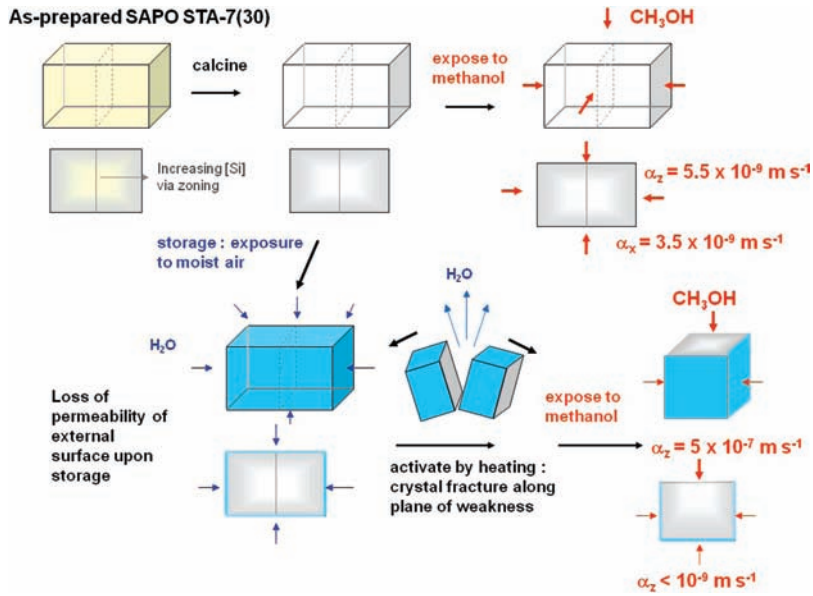

Figure 5. Schematical depiction of the physicochemical changes assumed to take place when a freshly calcined crystal of SAPO(30) STA-7 is exposed to methanol (upper part of the figure) or stored over several months followed by activation (leading to fracturing at a plane of weakness) and subsequently exposed to methanol (bottom part of the figure). Surface diffusivities measured by IFM are indicated. The defect plane is also illustrated.

estimate of the bulk diffusivity of the solid with higher Si content made from the fractured halves confirms that diffusion is much slower through SAPO(30) than within SAPO(10).

We speculate that the origin of this composition-dependent permeability and diffusivity is attributable to the higher concentration of strong adsorption sites (Brønsted hydroxyl groups) within the silicon-rich material, which are formed after the substitution of phosphorus by all the incorporated silica.[9] Such strong adsorption sites would retard the diffusion at room temperature, or to the presence of defects that form upon calcination in surface layers of very high Si/Al ratio that could result in strong adsorption sites or pore blockage.

The method also highlights the anomalous behavior of fracturing in those samples with high silica content that are stored in the calcined form and activated just prior to examination. During this procedure, internal tensions lead to crystal fracture into two halves along planes of weakness already present after synthesis, with a permeability of the evolving fractured face exceeding the permeability of the genuine crystal faces by more than 2 orders of magnitude! By keeping the sample in its as-synthesized form (i.e., under the stabilizing influence of the organic template) and by calcining only immediately before the onset of the sorption experiments, crystal fracture can be avoided. Surface permeabilities of the "genuine" crystal faces after storage as the calcined form and subsequent activation are smaller than the permeabilities of samples calcined immediately before measurement ($\alpha^{\text{fragment}}_{(30)z,\text{genuine}} < \alpha_{(30)z}$). Similarly, the diffusivities in SAPO STA-7 after storage as the calcined form ($D^{\text{fragment}}_{(30)z} \approx 6.7 \times 10^{-14}$ m^2 s^{-1}) are smaller than the diffusivities of samples calcined immediately before measurement ($D_{(30)z} \approx 1.6 \times 10^{-13}$ m^2 s^{-1}).

We hypothesize that calcination removes the template, which diffuses out, generating Brønsted acid sites due to the substitution of Si for P. Upon storage of the calcined form, adsorption of water results in some reduction in the crystallinity in the higher silica surface layers, which will have a higher concentration of Brønsted sites; this could result in acid hydrolysis of the local framework. It is possible that locally aluminosilicate regions with low Si/Al ratios form, which are known to be unstable under acid conditions. Solid state NMR reveals the presence of a significant amount of extra-framework aluminum in calcined SAPO(30) crystals allowed to rehydrate over several months (Supporting Information). This adsorption of moisture at the surface has the effect of decreasing the surface permeability below that of the freshly calcined material. Upon heating the sample to remove water, the internal pressure built up cannot quickly be released through this surface, resulting in fracture at the plane of weakness that is already present. This gives a permeable surface that slices through the center of the crystalline STA-7 framework. This resultant fractured surface has a lower Si content than that at the original external surface, due to zoning during crystallization, and so has a much higher permeability.

The effect of different procedures of calcination, storage, and activation on surface permeabilities of strongly zoned SAPO(30) crystals is illustrated schematically in Figure 5.

Conclusions

In summary, by analyzing the evolution of the guest profiles in SAPO STA-7 crystals in transient sorption experiments, we have shown that interference microscopy may readily be used to investigate more complex correlations, such as this of the transport resistances of the host material and the synthesis and/or pretreatment conditions. It was found that, by increasing the Si/(Al + Si + P) fraction of the framework from 0.09 to 0.185, both the intracrystalline diffusivities and especially the permeabilities through the outer surface of the host crystals decrease dramatically. Storage of the calcined Si-rich sample in ambient atmosphere gives rise to substantial loss of surface permeability which, upon sample activation, leads to crystal fracture. The permeability through the fracture face is found to be intermediate between the permeabilities through the other ("genuine") faces of the Si-rich sample and the faces of the sample with the low Si content, in line with selected area analyses that show strong compositional zoning in the crystals, such that the fractured surface will cut through framework with a range of Si/Al ratios.

The rate of guest transport within nanoporous materials is among the key parameters determining their technological utility. In particular, the effect on diffusion of the framework

composition and also the chemical zoning in SAPO catalysts prepared from gels with high Si contents that is observed here could lead to slow surface diffusion and deleterious effects on their performance in catalytic or adsorptive processes. With its unprecedented facility to quantify these parameters, interference microscopy has the potential to become an indispensable tool in the exploration of preparation and activation routes toward transport-optimized nanoporous materials.

Acknowledgment. The authors would like to thank the European Commission FP6Marie Curie Research Training Network 'INDENS' (MRTN-CT-2004-005503). Financial support by the German Science Foundation (International Research Training Group "Diffusion in Porous Materials") is also gratefully acknowledged. We thank the EPSRC solid state NMR facility, Durham University, for the NMR spectra and Julie Nairn (St. Andrews) for sample preparation.

Supporting Information Available: Experimental interference microscopy method, including algorithms and fits to the concentration profiles; table with transport parameters; MAS NMR results and complete ref 4. This material is available free of charge via the Internet at http://pubs.acs.org.

JA104016N